

PROPAGATION OF ULTRA-HIGH ENERGY COSMIC RAYS ABOVE 10^{19} EV IN A STRUCTURED EXTRAGALACTIC MAGNETIC FIELD AND GALACTIC MAGNETIC FIELDHAJIME TAKAMI¹, HIROYUKI YOSHIGUCHI¹ AND KATSUHIKO SATO^{1,2}
takami@utap.phys.s.u-tokyo.ac.jp
UTAP-529

ABSTRACT

We present numerical simulations on propagation of Ultra-High Energy Cosmic Rays (UHECRs) above 10^{19} eV in a structured extragalactic magnetic field (EGMF) and simulate their arrival distribution at the earth. We use the IRAS PSCz catalogue in order to construct a model of the EGMF and source model of UHECRs, both of which reproduce the local structures around the Milky Way. We also consider modifications of UHECR arrival directions by the Galactic magnetic field. We follow an inverse process of their propagation from the earth and record the trajectories. This enables us to calculate only trajectories of UHECRs arriving at the earth, which saves the CPU time. We construct arrival distribution of UHECRs from these trajectories and calculate the harmonic amplitudes and the two point correlation functions of their arrival distribution using our source models. We estimate number density of sources which explains the Akemo Ground Air Shower Array observation best. As a result, we find that $\sim 5 \times 10^{-6}$ Mpc⁻³ is the most appropriate number density of source of UHECRs, which constrains the source candidates of UHECRs. We also demonstrate skymaps of their arrival distribution with the event number expected by future experiments and examine how the EGMF affects their arrival distribution. The main result is diffusion of clustering events which are obtained by calculations neglecting the EGMF. Quantitatively, the EGMF weakens the peak of the two point correlation function at small angle scale and we find this fact explains the observational data better.

Subject headings: cosmic rays — methods: numerical — IGM: magnetic fields — galaxies: general — large-scale structure of the universe

1. INTRODUCTION

The nature of Ultra-High Energy Cosmic Rays (UHECRs), which are particles of energy above 10^{19} eV, is poorly known. This is one of the most challenging problems of modern astrophysics.

One of problems about UHECRs is what their origin is. The two scenarios of their origin are suggested, which are called top-down and bottom-up ones. On the one hand, bottom-up scenarios assume some astrophysical phenomena as their origin. UHECRs are thought to be of extragalactic origin since the gyroradii of UHECRs above 10^{19} eV exceed thickness of our galaxy. From this fact and the Hillas plot (Hillas 1984), their probable candidates are active galactic nuclei (AGNs), gamma-ray bursts (GRBs) and colliding galaxies. Theoretically, this scenario predicts the GZK effect (Greisen 1966; Zatsepin & Kuz'min 1966) since these source candidates of UHECRs are located at a far distance. UHE protons with energy above $\sim 8 \times 10^{19}$ eV interact with the cosmic microwave background (CMB) and lose large fraction ($\sim 20\%$) of their energy per interaction by photopion production (Berezinsky & Grigorieva 1988; Yoshida & Teshima 1993). The mean free path of UHE protons through the CMB field is ~ 10 Mpc at 10^{20} eV. Thus the energy spectrum at the Earth should have a cut-off around $E \sim 8 \times 10^{19}$ eV. This spectral cutoff is called the GZK cutoff. But there is a observational disagree of the energy spectra between the Akemo Giant Air Shower Array (AGASA), which does not observe the GZK cutoff (Takeda et al. 1998), and the High Resolution Fly's Eye (HiRes; Wilkinson et al. 1999), which does it (Abu-Zayyad et al. 2004). This discrepancy between the two experiments remains being one of open

questions in astroparticle physics. On the other hand, top-down scenarios assume some processes based on new physics beyond the standard model of the particle physics (see a review Bhattacharjee, P. & Sigl, G. (2000)).

Another problem is arrival distribution of UHECRs. The AGASA reported that there is no statistically significant large scale anisotropy in the observed arrival distribution of UHECRs above 10^{19} eV (Takeda et al. 1999). This fact points out that sources of UHECRs are distributed isotropically, but isotropic distribution of sources cannot explain the small-scale anisotropy reported by the AGASA (Takeda et al. 1999, 2001). A models of UHECR origin are constrained by their ability to reproduce such observed arrival distribution of UHECRs. On the other hand, the HiRes experiment indicates that there is no statistically significant small-scale anisotropy (Abbasi et al. 2004; Farrar et al. 2004). However Yoshiguchi et al. (2004) concluded this discrepancy between the two observations is not statistically significant at present. This problem is left for future investigation by new experiments such as the Pierre Auger Observatory.

To obtain information on UHECR origin, we need to calculate their arrival distribution using some kinds of source models. To do so, we have to simulate propagation of UHECRs in the intergalactic space, where the Extragalactic Magnetic Field (EGMF) plays important roles since we assume that UHECRs are protons in this paper. Yoshiguchi et al. (2003a) calculated propagation of UHE protons in an uniform turbulence of magnetic field with the Kolmogorov spectrum. But such magnetic field is not realistic since the EGMF is expected to reflect the large scale structure of the universe.

In recent years, several groups started to develop physically

¹ Department of Physics, School of Science, the University of Tokyo, 7-3-1 Hongo, Bunkyo, Tokyo 113-0033, Japan² Research Center for the Early Universe, School of Science, the University of Tokyo, 7-3-1 Hongo, Bunkyo, Tokyo 113-0033, Japan

more realistic models of the EGMF based on numerical simulations of large scale structure formation. Sigl, Miniati, & Ensslin (2003, 2004) used a structured EGMF model which is generated by their large scale structure simulations, taking magnetic fields into account. But their model does not reproduce the local structures actually observed around the Milky Way. This causes the ambiguity in the choice of observer position. In addition to this, the calculated arrival distribution of UHECRs does not correspond to the one expected at the earth.

An important step on modeling the magnetic structure of the local universe is performed by Dolag et al. (2005). They constrain the initial conditions for the dark matter density fluctuations to reproduce the local structures around the Milky Way. This allows us to remove the ambiguity in the choice of observer position, and to obtain the simulated sky maps of expected UHE proton deflections in the magnetic large-scale structure around the Milky Way. However, they do not calculate the arrival distribution of UHECRs, and thus cannot obtain the information on source distribution which reproduces the AGASA observation. And also, the effects of the Galactic Magnetic Field (GMF) are not considered in both Sigl, Miniati, & Ensslin (2003, 2004) and Dolag et al. (2005). But recently it has also been shown that the GMF affects the arrival distribution of UHECRs (Alvarez-Muniz, Engel & Stanev 2002; Yoshiguchi et al. 2003b). Thus we cannot neglect modifications of arrival directions of UHECRs by the GMF when we simulate their arrival distribution.

In this work, we calculate propagation of UHECRs taking the EGMF and the GMF into account, following their trajectories and simulate the arrival distribution of UHECRs. We compare the results with the AGASA observation. We generate the magnetic structure of the local universe by our original method (section 3.1) using the IRAS PSCz catalogue of galaxies (Saunders et al. 2000). We also construct our source models of UHECRs from this catalogue. As our GMF model, we adopt a bisymmetric spiral field (BSS) model (Alvarez-Muniz, Engel & Stanev 2002) just like Yoshiguchi et al. (2003b).

In order to simulate the arrival distribution of UHECRs, we apply a method developed in previous works. (Flückiger et al. 1991; Bieber, Evenson, & Lin 1992; Stanev 1997; Medina-Tanco 1999; Yoshiguchi et al. 2003b). We numerically calculate an inverse process of propagation of UHE protons, which reach the earth, and record their trajectories in our Galaxy and the intergalactic space. In other words, we inject UHECRs from the earth isotropically whose charges are taken as -1. We then select some of them according to a given source distribution. (Detailed explanation is given in the section 4.3) The expected arrival distribution can be obtained by mapping the velocity directions of the selected trajectories at the earth. The validity of this method is supported by the Liouville's theorem. This method enables us to save the CPU time effectively since we calculate only trajectories of protons which reach the earth. A method for this process is explained in section 4

The outline of this paper is as follows. In section 2, we explain the IRAS PSCz Catalogue and construct our sample of galaxies. In section 3, we introduce our model of the EGMF and the GMF. We explain our numerical methods for calculating arrival distribution of UHECRs and statistical quantities in section 4. Then in section 5, we estimate the most appropriate number density of source of UHECRs and compare the statistical quantities calculated using this source model with the EGMF with those calculated without the EGMF. We also

demonstrate skymaps of the arrival distribution of UHECRs. In section 6, we summarize the main results.

2. A SAMPLE OF GALAXIES

In order to calculate propagation of UHECRs considering the local structures actually observed around the Milky Way, we use the IRAS PSCz Catalogue (Saunders et al. 2000).

We used the ORS sample to construct our UHECR source models in our previous work (Yoshiguchi et al. 2003a). The ORS galaxy sample has better completeness on nearby galaxies than the IRAS PSCz catalogue. Thus we used the ORS sample since we were interested in the local sources in order to research nature of UHECRs above 4×10^{19} eV. Then we investigated that this source model also explained arrival distribution of UHECRs above 10^{19} eV though the EGMF was neglected (Yoshiguchi et al. 2003b). But in this work, we use galaxy sample to construct not only a source model of UHECRs but also a model of the EGMF, which reflects the large scale structure of the universe. This requests large sky coverage of galaxy survey project. Thus we adopt not the ORS galaxy catalogue but the IRAS PSCz Catalogue.

The IRAS PSCz catalogue consists of 14677 galaxies with redshift and infrared fluxes > 0.6 Jy, and covers about 84% of the sky. We assume de Sitter universe with $\Omega_m = 0.3, \Omega_\lambda = 0.7, H_0 = 71 \text{ km s}^{-1} \text{ Mpc}^{-1}$ in order to calculate distance of each galaxy. We show distribution of the IRAS PSCz galaxies in Figure 1.

However, there are two problems when we use the IRAS PSCz Catalogue in this work. One is that the more distant galaxies we observe, the more difficult we find it to observe dark galaxies (the selection effect, see Figure 2). The other is that this catalogue have the zone of avoidance (the mask), where the IRAS PSCz Survey did not observe. Our previous works (Yoshiguchi et al. 2003a,b), which uses the ORS sample (Santiago et al. 1995), also have these problems. Using luminosity function, we correct these absence of galaxies in the same manner with our previous study.

We use the luminosity function of the IRAS PSCz galaxies (Takeuchi et al. 2003)

$$\Phi(L) = \phi_* \left(\frac{L}{L_*} \right)^{1-\alpha} \exp \left\{ -\frac{1}{2\sigma^2} \left[\log \left(1 + \frac{L}{L_*} \right) \right]^2 \right\}. \quad (1)$$

Here $L_* = (4.34 \pm 0.86) \times 10^8 h^{-2} [L_\odot]$, $\alpha = 1.23 \pm 0.04$, $\sigma = 0.724 \pm 0.010$, $\phi_* = (2.34 \pm 0.30) \times 10^{-2} h^3 \text{Mpc}^3$. We introduce the selection function,

$$\phi(r) = \frac{\int_{L_{\min(r)}}^{\infty} dL \Phi(L)}{\int_0^{\infty} dL \Phi(L)} \quad (2)$$

where $L_{\min(r)}$ is minimum luminosity of galaxies which are observable at distance r . Therefore, $\phi(r)$ represents the fraction of all galaxies that are observable at each r .

First of all, we correct the selection effect. For each of the IRAS galaxies, we add galaxies that are not included in the IRAS sample by using the selection function. The positions of added galaxies are determined according to a Gaussian distribution whose mean is the position of the original IRAS galaxy and whose root mean square is $l(r)$. Here we define $l(r)$ as a mean distance between the original IRAS galaxies, thus

$$\frac{4\pi}{3} l(r)^3 n(r) = 1, \quad (3)$$

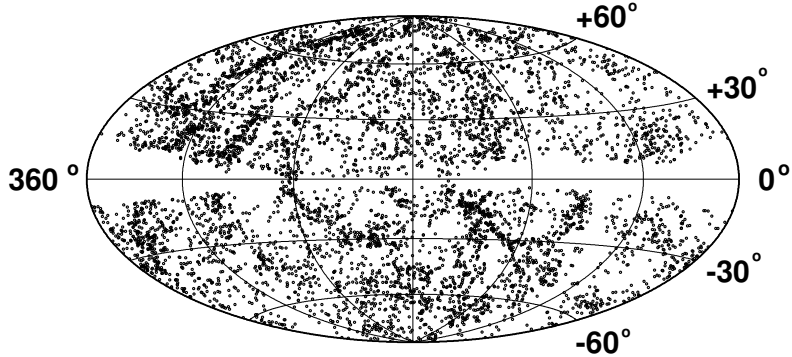


FIG. 1.— The IRAS PSCz galaxies on the galactic coordinate. Strong infrared luminosity on the galactic plane interrupt observation of galaxies near the galactic plane.

where $n(r)$ is number density of the original IRAS galaxies. Then,

$$l(r) = \left(\frac{3}{4\pi} \right)^{1/3} n(r)^{-1/3}. \quad (4)$$

The luminosities of added galaxies are randomly assigned so that their distribution is consistent with the luminosity function. This method for correction can complement galaxies without spoiling the observed structure of galaxy distribution.

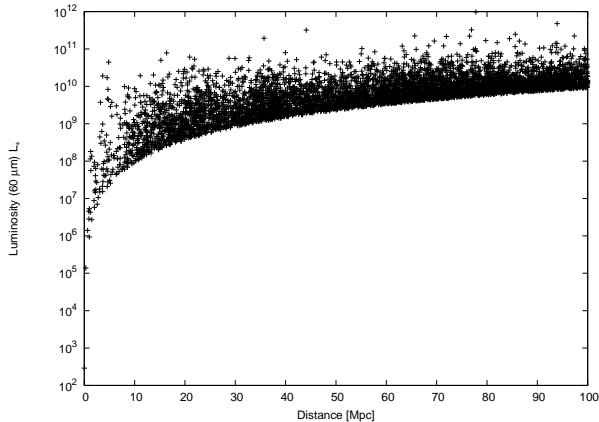


FIG. 2.— Infrared luminosity ($60\mu\text{m}$) of the IRAS PSCz galaxies plotted as a function of distance from the Earth. Unit of luminosity is L_\odot .

Next, we add galaxies in the mask. We assume that the galaxy distribution in this region is homogeneous and number density of galaxies is $n(r)/\phi(r)$. These luminosities are random but their distribution is consistent with the luminosity function. Our galaxy sample with these corrections is shown in Figure 3.

In this work, in order to construct our sample of galaxies we use only the IRAS galaxies within 100 Mpc. We assume that distribution of sources at $r > 100$ Mpc is isotropic and uniform,

and that their number density is equal to that within 100 Mpc. Thus our sample of galaxies reflects observed local structure at only $r < 100$ Mpc.

We use this sample of galaxies to construct a model of extra-galactic magnetic fields and source model of UHECRs.

3. A MODEL OF MAGNETIC FIELD

3.1. *Extragalactic Magnetic Field*

The EGMF are little known theoretically and observationally. Theoretically, several large scale structure simulations with magnetic field have been performed (Dolag et al. 2005; Sigl, Miniati, & Ensslin 2004). Roughly speaking, their results are that the strength of magnetic field traces baryon density. A model of Sigl, Miniati, & Ensslin (2004) do not reflect the local structures actually observed around the Milky Way, while one of Dolag et al. (2005) reflects these local structures. To compare model predictions of UHECR arrival distribution with the observation, it is important to generate the magnetic structure around the Milky Way. Therefore, we present a model of the EGMF reflecting the local structures of the universe well.

The EGMF mainly exists in clusters of galaxy or around galaxies. From this standpoint, we present a realistic model of the EGMF. We assume that magnetic field results from the amplification of weak seed fields. In a simulation of evolution of cluster of galaxy (Dolag et al. 2002), the average magnetic field strength in the cluster is amplified as expected from compression alone ($|B| \propto \rho^{3/2}$, where ρ is density of matter). We adopt this conclusion

$$|B| \propto L^{2/3}. \quad (5)$$

Here we assume that luminosity of each galaxy is proportional to density of gas. With these assumption, we construct a model of the EGMF as follows.

First, we cover the universe with cubes of side l_c , which is correlation length of the EGMF. We adopt $l_c = 1\text{Mpc}$ from our

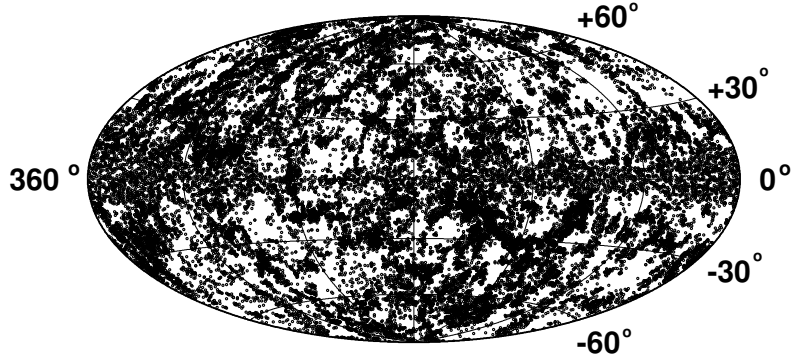


FIG. 3.— Distribution of galaxies after correction for the selection effect and existance of the mask. This distribution do not spoil the observed structure of galaxy distribution.

previous work (Yoshiguchi et al. 2003a). Second, we sum luminosities of galaxies in our sample which exist in each cube. We call this summed value luminosity density. The L in the equation 5 is luminosity density. Finally, we assume that the magnetic field in each cube is represented as the Gaussian random field with zero mean and a power-law spectrum. Thus,

$$\begin{aligned} \langle B(\vec{k})B^*(\vec{k}) \rangle &\propto k^{n_H} \quad \text{for } 2\pi/l_c \leq k \leq 2\pi/l_{\text{cut}}, \\ \langle B(\vec{k})B^*(\vec{k}) \rangle &= 0 \quad \text{otherwise,} \end{aligned} \quad (6)$$

where l_{cut} is a numerical cutoff scale. Physically, one expects $l_{\text{cut}} \ll l_c$, but we set $l_{\text{cut}} = 1/8 \times l_c$ in order to save the CPU time. We use $n_H = -11/3$, corresponding to the Kolmogorov spectrum since the Faraday rotation map reveals that the clusters' magnetic fields are turbulent with the Kolmogorov spectrum over at least one order of magnitude (Vogt, C & Ensslin, T.A. 2004).

Next we consider the normalization of the EGMF. Most observations suggest that clusters of galaxy have magnetic field whose strength is from $0.1 \mu\text{G}$ to a few μG (see a review Vallee (2004)). On the one hand, Faraday rotation measurements of polarized radio sources placed within cluster of galaxies provide evidence for the presence of stronger intracluster magnetic field (ICMF), in the range of a few μG (Taylor et al. 2001; Vogt et al. 2003). On the other hand, the observation of hard X-ray emission from cluster of galaxy implies an average ICMF strength within the emitting volume in the range of $0.2\text{--}0.4 \mu\text{G}$ (Fusco-Femiano et al. 1999; Rephaeli et al. 1999). In this work, we now set a normalization of its strength $\sim 0.4 \mu\text{G}$ in a cube where is the center of the Virgo cluster. We show magnetic field strength along three fiducial lines through the Virgo cluster, the Perseus cluster and the Coma cluster within 100 Mpc in figure 4 in order to compare our model with Dolag et al. (2005).

We use our sample of galaxy to construct a model of the EGMF within 100 Mpc. At a distance above 100 Mpc, we treat the EGMF as an uniform turbulence of magnetic field with the

same spectrum and $|B| = 1 \text{ nG}$ since the IRAS PSCz catalogue is poorly covered at $r > 100 \text{ Mpc}$.

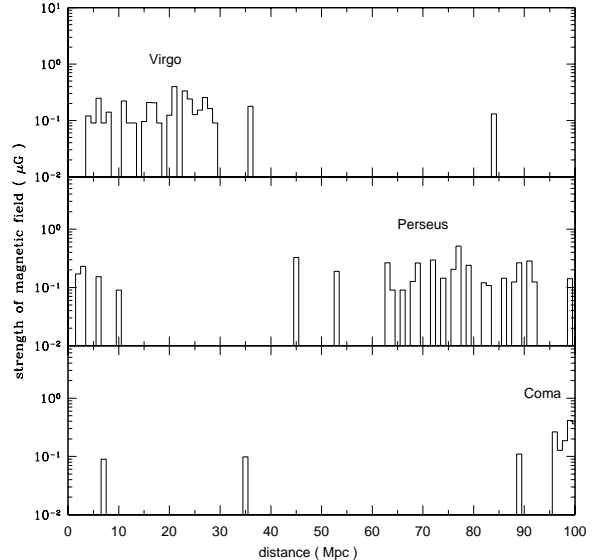


FIG. 4.— Magnetic field strength along three fiducial lines through the Virgo cluster, the Perseus cluster and the Coma cluster within 100 Mpc.

3.2. Galactic Magnetic Field

In this study, we adopt the GMF model used by Alvarez-Muniz, Engel & Stanev (2002), which is composed of the spiral and the dipole field. We briefly explain this GMF model below.

Faraday rotation measurements indicate that the GMF in the disk of the Galaxy has a spiral structure with field reversals at the optical Galactic arms (Beck 2001). We use a bisymmetric

spiral field (BSS) model, which is favored from recent work (Han, Manchester, & Qiao 1999; Han 2001). The Solar System is located at a distance $r_{||} = R_{\oplus} = 8.5$ kpc from the center of the Galaxy in the Galactic plane. The local regular magnetic field in the vicinity of the Solar System is assumed to be $B_{\text{Solar}} \sim 1.5 \mu\text{G}$ in the direction $l = 90^\circ + p$ where the pitch angle is $p = -10^\circ$ (Han & Qiao 1994).

In the polar coordinates $(r_{||}, \phi)$, the strength of the spiral field in the Galactic plane is given by

$$B(r_{||}, \phi) = B_0 \left(\frac{R_{\oplus}}{r_{||}} \right) \cos \left(\phi - \beta \ln \frac{r_{||}}{r_0} \right) \quad (7)$$

where $B_0 = 4.4 \mu\text{G}$, $r_0 = 10.55$ kpc and $\beta = 1/\tan p = -5.67$. The field decreases with Galactocentric distance as $1/r_{||}$ and it becomes zero for $r_{||} > 20$ kpc. In the region around the Galactic center ($r_{||} < 4$ kpc) the field is highly uncertain, and thus assumed to be constant and equal to its value at $r_{||} = 4$ kpc.

The spiral field strengths above and below the Galactic plane are taken to decrease exponentially with two scale heights (Stanev 1997)

$$|B(r_{||}, \phi, z)| = |B(r_{||}, \phi)| \begin{cases} \exp(-z) : & |z| \leq 0.5 \text{ kpc} \\ \exp(-\frac{z}{8}) \exp(-\frac{z}{4}) : & |z| > 0.5 \text{ kpc} \end{cases} \quad (8)$$

where the factor $\exp(-3/8)$ makes the field continuous in z . The BSS spiral field we use is of even parity, that is, the field direction is preserved at disk crossing.

Observations show that the field in the Galactic halo is much weaker than that in the disk. In this work we assume that the regular field corresponds to a A0 dipole field as suggested in (Han 2002). In spherical coordinates (r, θ, φ) the (x, y, z) components of the halo field are given by:

$$\begin{aligned} B_x &= -3 \mu_G \sin \theta \cos \theta \cos \varphi / r^3 \\ B_y &= -3 \mu_G \sin \theta \cos \theta \sin \varphi / r^3 \\ B_z &= \mu_G (1 - 3 \cos^2 \theta) / r^3 \end{aligned} \quad (9)$$

where $\mu_G \sim 184.2 \mu\text{G kpc}^3$ is the magnetic moment of the Galactic dipole. The dipole field is very strong in the central region of the Galaxy, but is only $0.3 \mu\text{G}$ in the vicinity of the Solar system, directed toward the North Galactic Pole.

There is a significant turbulent component, B_{random} , of the Galactic magnetic field. Its field strength is difficult to measure and results found in literature are in the range of $B_{\text{random}} = 0.5 \dots 2 B_{\text{reg}}$ (Beck 2001). However, we neglect the random field throughout the paper. Possible dependence of the results on the random field is discussed in the section 5.

4. NUMERICAL METHOD

4.1. Method of Calculation for Propagation of UHECRs

This subsection provides our method of simulation for propagating protons in the intergalactic space. We expand a method of calculation in our previous work (Yoshiguchi et al. 2003b).

In this study, we calculate arrival distribution of UHE protons applying the method developed in previous works (Flückiger et al. 1991; Bieber, Evenson, & Lin 1992; Stanev 1997; Medina-Tanco 1999; Yoshiguchi et al. 2003b). We numerically calculate inverse process of propagation of UHE protons, which arrive at the earth, and record their trajectories in our Galaxy and the intergalactic space. We then select some of them according to a given source distribution. (Detailed explanation is given in the section 4.3) The expected arrival distribution can be obtained by mapping the velocity directions of the selected trajectories at the earth. The validity of this method is supported by Liouville's theorem.

We already performed numerical simulations for UHECR propagation in the GMF in Yoshiguchi et al. (2003b). We injected UHECRs from the earth isotropically, and recorded these trajectories until they reached a sphere of radius 40 kpc centered at the galactic center. The charge of UHECRs was taken as -1 because we followed propagation of UHE protons backward. These UHECRs were injected with spectral index of -2.7 , which was similar to observed one. Note that this is not the energy spectrum injected at extragalactic sources.

In this study, we extend these trajectories in our Galaxy to the extragalactic space. The trajectories are followed until their distance from our Galaxy reach 1 Gpc or their time for propagation reach the age of the universe. Of course, we set the charge of UHECRs to be -1 .

In the extragalactic space, we have to consider not only the deflections due to magnetic fields but also the energy loss process (Berezinsky & Grigorieva 1988; Yoshida & Teshima 1993). UHE protons below 8×10^{19} eV lose their energies mainly by adiabatic energy losses and pair creations in collision with photons of the CMB, and above it by photopion production with the CMB photons. Though we assume that UHECRs are protons in this work, we should also add the photodisintegration if we assume UHECRs to be nuclei. We treat all these energy loss process as a continuous process. Note that energies of UHECRs increase during propagation because we follow their inverse processes.

The adiabatic energy loss is the effect of the expanding universe. This energy loss is written

$$\dot{E} = -\frac{\dot{a}}{a} E = -H_0 [\Omega_m (1+z)^3 + \Omega_{\Lambda}] E. \quad (10)$$

As mentioned in section 2, the cosmological parameters used in this calculation are $\Omega_m = 0.3$, $\Omega_{\Lambda} = 0.7$, and $H_0 = 71 \text{ km s}^{-1} \text{ Mpc}^{-1}$.

The pair production due to collisions with the CMB can be treated as a continuous process considering its small inelasticity ($\sim 10^{-3}$). We adopt the analytical fit functions given by Chodowski, Zdziarske, & Sikora (1992) to calculate the energy loss rate for the pair production on isotropic photons. The same approach has been adopted in our previous studies (Yoshiguchi et al. 2003a,b).

UHE protons above $\sim 8 \times 10^{19}$ eV lose a large fraction of their energy ($\sim 20\%$ at every reaction) in the photopion production. We treated this process as a stochastic process in previous work (Yoshiguchi et al. 2003b). But in this study, we cannot treat this as a stochastic process because we expand our previous method of calculating propagation of UHECRs — we calculate an inverse process (see Yoshiguchi et al. (2003b) or Section 4.1) —. Aloisio & Berezinsky (2004) showed that the energy spectrum which is calculated with a continuous process of photopion production is consistent with the one calculated with a stochastic process if a distance between the earth and sources of UHECR is more than 30 Mpc. Thus, we can adopt a continuous energy loss process since our source model (explained below) fully satisfy that condition about distances of sources. We use the energy loss length which is calculated by simulating the photopion production with the event generator SOPHIA (Mucke et al. 2000).

4.2. Source Distribution

We construct source models of UHECRs from our sample of galaxies. The number density of UHECR sources is taken as our model parameter. For a given number density, we randomly select galaxies from our sample with probability proportional to absolute luminosity of each galaxy. We then estimate the source number density which reproduces the observed arrival distribution of UHECRs, by calculating the harmonic amplitude and the two point correlation function of arrival distribution of UHECRs as a function of the source number density.

4.3. Calculation of the UHECR Arrival Distribution

In this subsection, we explain the method of construction of UHECR arrival distribution at the earth. We calculate and record 500,000 trajectories of UHE protons in the EGMF, using our method explained in Section 4.1. We use these trajectories to construct the arrival distribution of UHECRs as follows.

First, we distribute our sources of UHECR in the universe. Second, we calculate quantities to every trajectory of UHECR, which are

$$P_{\text{selec}}(E, j) \propto \sum_i \frac{L_{i,j}}{d_{i,j}^2} \frac{dN/dE(d_{i,j}, E_i)}{E^{-2.7}}. \quad (11)$$

Here, i labels sources on each trajectory. $d_{i,j}$ and $L_{i,j}$ is a distance and luminosity of each source which is passed by j th proton respectively. $dN/dE(d_{i,j}, E_i)$ is the energy spectrum of protons injected at a source of distance $d_{i,j}$. E_i is energy of proton at i th source. $P_{\text{selec}}(E, j)$ represents a relative probability that j th proton reaches the Earth. We randomly select several trajectories according to these relative probabilities, so that the number of the selected trajectories is equal to the observed event number. The mapping of the velocity directions of each UHECR at the earth becomes the arrival distribution of UHECRs. If we have to select the same trajectory more than once in order to adjust the number of the selected trajectories, we generate a new event whose arrival angle is calculated by adding a normally distributed deviate with zero mean and variance equal to the experimental resolution 2.8° (1.8°) for $E > 10^{19}$ eV (4×10^{19} eV) to the original arrival angle.

We assume that UHECRs are protons injected with a power law spectrum in the range of $10^{19} - 10^{22}$ eV. We set this power law index 2.6 in order to fit the calculated energy spectrum to the one observed by the AGASA (Marco, Blasi, & Olinto 2003). In other words, $dN/dE(d_{i,j}, E) \propto E^{-2.6}$ where E is the energy of UHECR at the source.

4.4. Statistical Methods

In this subsection, we explain the two statistical quantities, the harmonics analysis for large scale anisotropy (Hayashida et al. 1999) and the two point correlation function for small scale anisotropy.

The harmonic analysis to the right ascension distribution of events is the conventional method to search for large scale anisotropy of cosmic ray arrival distribution. For a ground-based detector like the AGASA, the almost uniform observation in right ascension is expected. The m -th harmonic amplitude r is determined by fitting the distribution of cosmic rays to a sine wave with period $2\pi/m$. For a sample of n measurements of phase, $\phi_1, \phi_2, \dots, \phi_n$ ($0 \leq \phi_i \leq 2\pi$), it is expressed as

$$r = (a^2 + b^2)^{1/2} \quad (12)$$

where, $a = \frac{2}{n} \sum_{i=1}^n \cos m\phi_i$, $b = \frac{2}{n} \sum_{i=1}^n \sin m\phi_i$. We calculate the harmonic amplitude for $m = 1, 2$ from a set of events generated by the method explained in the section 4.3.

If events with total number n are uniformly distributed in right ascension, the chance probability of observing the amplitude $\geq r$ is given by,

$$P = \exp(-k), \quad (13)$$

where

$$k = nr^2/4. \quad (14)$$

The current AGASA 775 events above 10^{19} eV is consistent with isotropic source distribution within 90 % confidence level (Takeda et al. 2001). We therefore compare the harmonic amplitude for $P = 0.1$ with the model prediction.

The two point correlation function $N(\theta)$ contains information on the small scale anisotropy. We start from a set of events generated from our simulation. For each event, we divide the sphere into concentric bins of angular size $\Delta\theta$, and count the number of events falling into each bin. We then divide it by the solid angle of the corresponding bin, that is,

$$N(\theta) = \frac{1}{2\pi |\cos\theta - \cos(\theta + \Delta\theta)|} \sum_{\theta \leq \phi \leq \theta + \Delta\theta} 1 \text{ [sr}^{-1}], \quad (15)$$

where ϕ denotes the separation angle of the two events. $\Delta\theta$ is taken to be 1° in this analysis. The AGASA data shows correlation at small angle ($\sim 3^\circ$) with 2.3 (4.6) σ significance of deviation from an isotropic distribution for $E > 10^{19}$ eV ($E > 4 \times 10^{19}$ eV) (Takeda et al. 2001).

5. RESULTS

In this section, we present the results of simulations of the arrival distribution of UHECRs above 10^{19} eV, adopting the method explained in the section 4.3. In section 5.1, we find a constraint on source model. Then using the source model obtained in section 5.1, we see how the EGMF affects the arrival distribution of UHECRs in section 5.2 and section 5.3.

5.1. Constraint on source model of UHECRs

In this subsection, we constrain the source number density of UHECRs using the results of the arrival distribution.

Figure 5 and figure 6 show the harmonic amplitude simulated by our source models. The number of simulated events is set to be 775 in the energy above 10^{19} eV and their arrival direction is restricted in the range $-10^\circ \leq \delta \leq 80^\circ$ in order to compare our result with that of the AGASA. Note that δ is declination. The shaded regions represent 1σ total statistical error, which is caused by the two components of statistical error—the finite number of simulated events and the random source selections from our IRAS sample. In order to see magnitude of each error, we also draw an errorbar, which represents the only statistical fluctuations due to the finite number of the simulated events. The event selections and the random source selections are performed 100 times and 40 times respectively. The region below the histogram is expected for the statistical fluctuation of isotropic source distribution with the chance probability larger than 10%. Both first and second amplitudes, for all source number density, show that our source models predict sufficient isotropy of UHECR arrival distribution obtained by the AGASA.

Next, we investigate what number density of sources explain the two point correlation obtained by the AGASA best. In order to evaluate it, we introduce $\chi_{\theta_{\text{max}}}$ as

$$\chi_{\theta_{\text{max}}} = \frac{1}{\theta_{\text{max}}} \sqrt{\sum_{\theta=0}^{\theta_{\text{max}}} \frac{\{N(\theta) - N_{\text{obs}}(\theta)\}^2}{\sigma(\theta)^2}}, \quad (16)$$

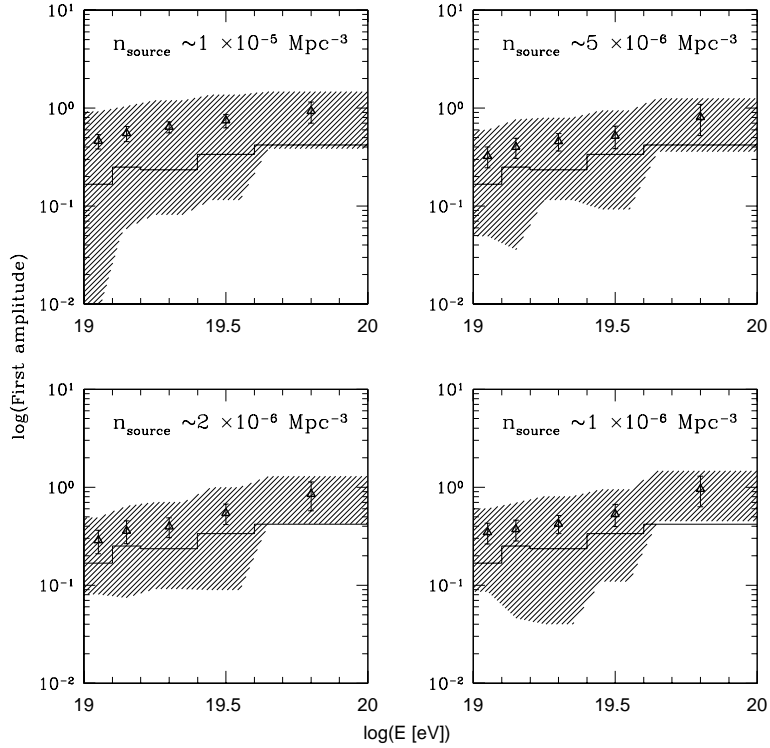


FIG. 5.—First amplitudes predicted by our source models, as a function of the cosmic ray energies. The shaded regions represent 1σ total statistical error due to the event selections and the source selections. The errorbars represent the statistical fluctuations only due to the event selections. The number of simulated events is set to be equal to that observed by the AGASA. The upper left is the first amplitude calculated by a source model whose number density of source n_{source} is $\sim 1 \times 10^{-5} \text{ Mpc}^{-3}$. The upper right, the lower left and the lower right are the first amplitudes for $n_{\text{source}} \sim 5 \times 10^{-6}, 3 \times 10^{-6}, 1 \times 10^{-6} \text{ Mpc}^{-3}$ respectively.

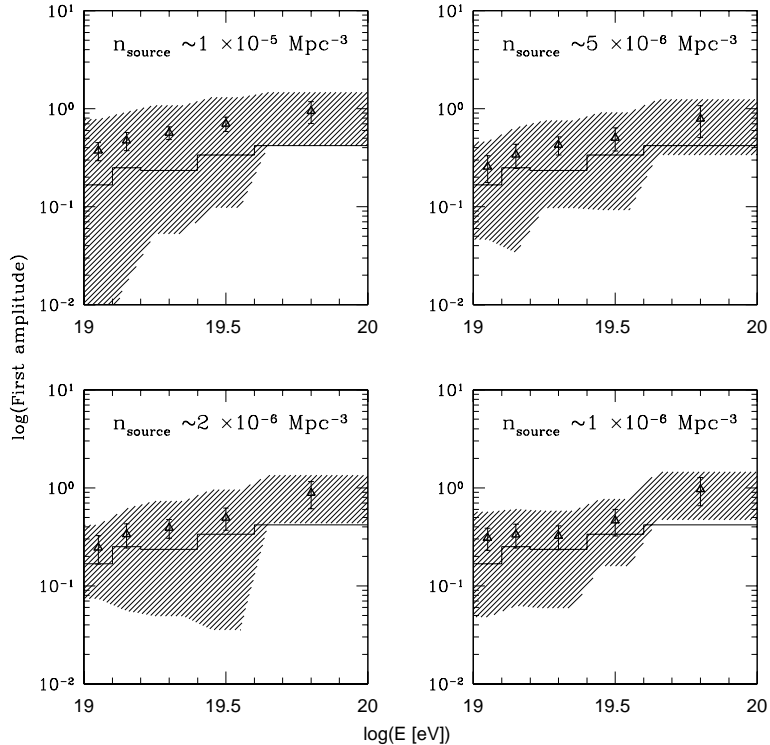


FIG. 6.—The same as Fig. 5, but for amplitude of the second harmonics.

where $N(\theta)$ is the two point correlation function calculated from simulated arrival distribution within $-10^\circ \leq \delta \leq 80^\circ$ and $N_{\text{obs}}(\theta)$ is that obtained from the AGASA data at angle θ . $\sigma(\theta)$ is statistical error of $N(\theta)$ due to the finite number of simulated events. The random event selection are performed 100 times. This $\chi_{10,\text{max}}$ represents goodness of fitting between the simulated two point correlation and the observed one. In this study, we take θ_{max} to be 10° .

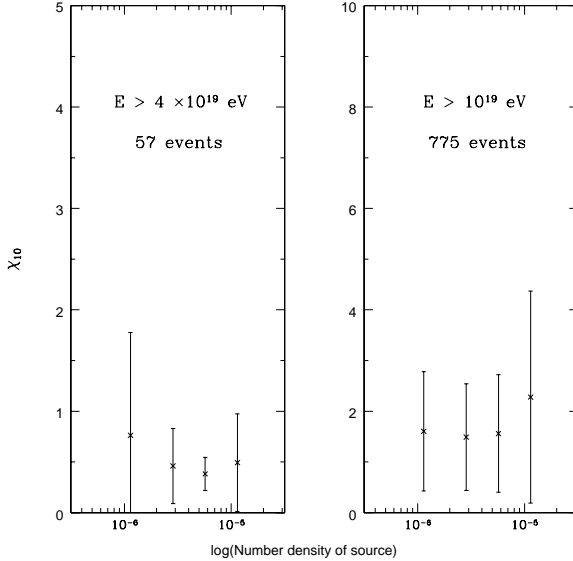


FIG. 7.— χ_{10} as a function of number density of source (n_{source}). The errorbars represent the statistical fluctuations due to the source selections from our galaxy sample. The left and right panel are calculated in the energy range of $E > 4 \times 10^{19}$ eV and $E > 10^{19}$ eV, respectively.

Figure 7 shows χ_{10} as a function of number density of source (n_{source}). The errorbars represent the statistical fluctuations due to the source selections from our galaxy sample. The random source selections are performed 40 times. The left and right panel are calculated in the energy range of $E > 4 \times 10^{19}$ eV and $E > 10^{19}$ eV, respectively. However, we cannot know the normalization of two point correlation function obtained from the AGASA for $E > 10^{19}$ eV. Thus, we fit the two point correlation function obtained by the AGASA data to that calculated from our simulation at θ_{max} .

In the right panel, three number density of source get similar χ_{10} value since distant sources ($r > 100$ Mpc) strongly contribute to arrival cosmic rays in the low energy range $E <$ a few $\times 10^{19}$ eV. χ_{10} calculated from a source model of $n_{\text{source}} \sim 10^{-5}$ Mpc $^{-3}$ is larger than the others. This is because this source model contains extremely near sources due to larger n_{source} . In the left panel, which is the result for higher energy cosmic rays, source number density affects strongly χ_{10} since near source ($r < 100$ Mpc) contribute to arrival ones due to the GZK effect. As is seen from the figure, $n_{\text{source}} \sim 5 \times 10^{-6}$ Mpc $^{-3}$ explains the two point correlation function obtained by the AGASA best.

Therefore, $n_{\text{source}} \sim 5 \times 10^{-6}$ Mpc $^{-3}$ is the most appropriate number density of UHECR source, since this source model also explains the harmonic amplitude obtained by the AGASA well. Note that number density of sources have some uncertainty since the error bars in both panels are large.

Figure 8 is the energy spectra at the earth predicted by our source models. These spectra are averaged ones 40 times of the

source selections on each source model. Solid line represents energy spectrum obtained for $n_{\text{source}} \sim 5 \times 10^{-6}$ Mpc $^{-3}$. We also show the observed cosmic-ray spectrum by the AGASA. These simulated energy spectra have cutoff around $E \sim 10^{19.6-8}$ eV, which are the GZK cutoff. These spectra can explain the AGASA data (Hayashida et al. 2000) below 10^{20} eV except a spectrum with $n_{\text{source}} \sim 1 \times 10^{-6}$ Mpc $^{-3}$. The most appropriate source model ($n_{\text{source}} \sim 5 \times 10^{-6}$ Mpc $^{-3}$) also explains the observed energy spectrum only below 10^{20} eV. We concluded in Yoshiguchi et al. (2003a) that a large fraction of cosmic rays above 10^{20} eV observed by the AGASA might be originate in the top-down scenarios. Thus we consider UHECRs with only $E < 10^{20}$ eV in what follows.

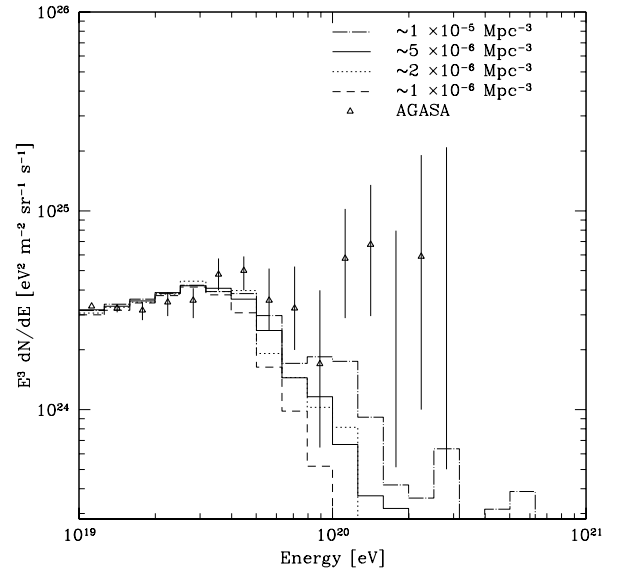


FIG. 8.— Energy spectra at the earth predicted by our source models. These spectra are averaged ones 40 times of the source selections on each source model. Solid line represents energy spectrum obtained by source model whose number density is $\sim 5 \times 10^{-6}$ Mpc $^{-3}$. We also show the observed cosmic-ray spectrum by the AGASA.

5.2. Arrival Distribution of UHECRs above 10^{19} eV

In this subsection, we demonstrate a skymap of the arrival distribution of UHECRs in the case of $n_{\text{source}} \sim 5 \times 10^{-6}$ Mpc $^{-3}$. We construct their arrival distribution using our method explained in the section 4.3.

We show one of results of the event generation above 10^{19} eV in figure 9 with a specific source model for $n_{\text{source}} \sim 5 \times 10^{-6}$ Mpc $^{-3}$. The points represent each event and the events are colored according to their energies. The number of events is 5000, which is the expected number of events observed by the Pierre Auger observatory for a few years (Capelle et al. 1998). The skymap generated with both the EGMF and the GMF is in the lower right panel and that without any magnetic fields, that with only the EGMF and that with only the GMF is in the upper left, the upper right and the lower left panel respectively.

This specific source model has three strong sources (see upper left). One is $(l, b) \sim (199^\circ, 34^\circ)$, another is $(l, b) \sim (287^\circ, 19^\circ)$ and the other is $(l, b) \sim (25^\circ, 11^\circ)$. Each distance from us is about 77 Mpc, 65 Mpc and 70 Mpc respectively.

In the absence of any magnetic fields (upper left panel), there are the strong clusterings of events at the directions of these

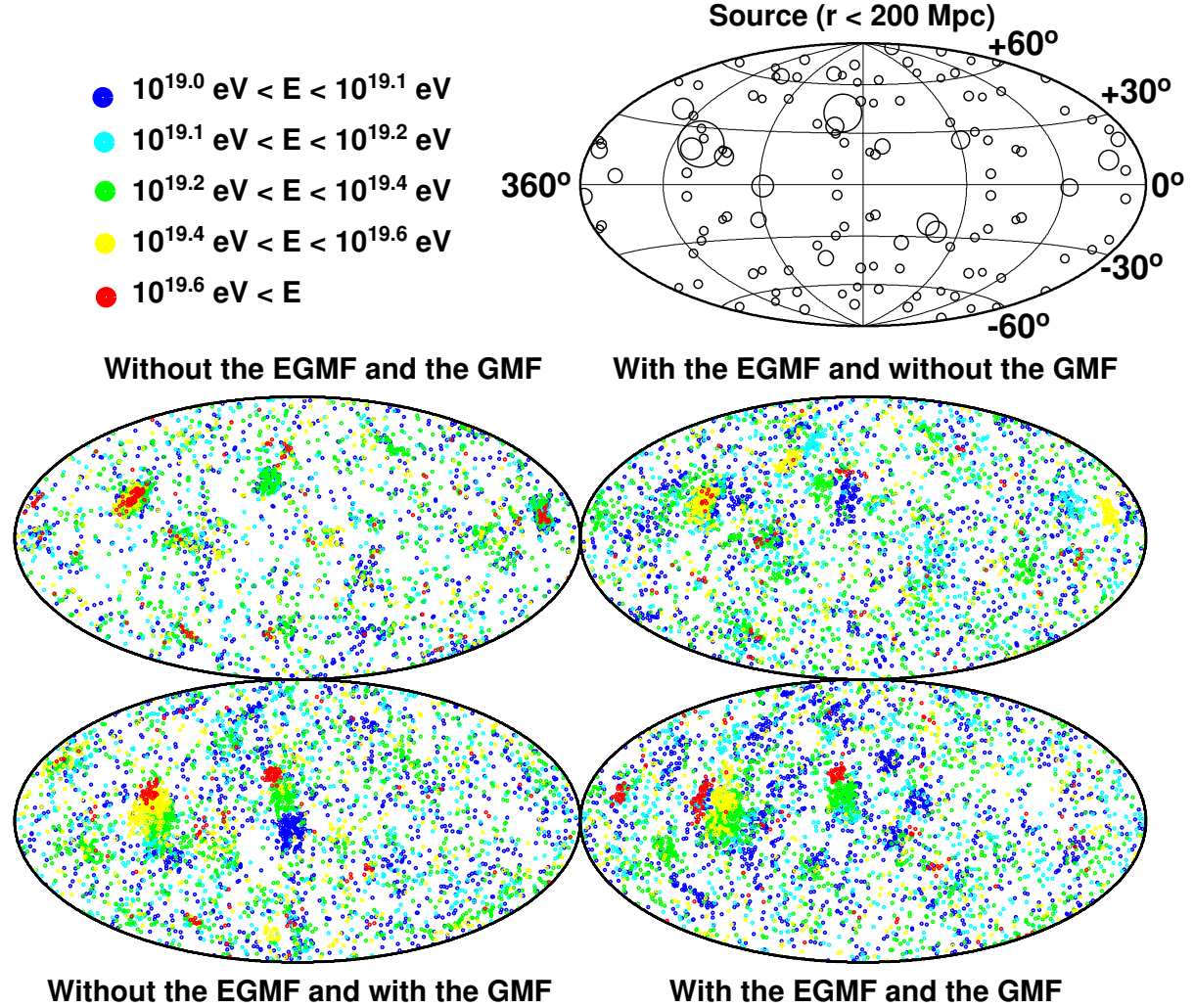


FIG. 9.— Skymaps of arrival distribution of UHE protons with $E > 10^{19}$ eV at the earth, which is expected for the source model of uppermost panel in the galactic coordinate. It is only the sources within 200 Mpc from us for clarity as circles of radius inversely proportional to their distances. The events are shown by color according to their energies. The event number is 5000, which is the expected number of event observed by the Pierre Auger observatory (Capelle et al. 1998) for a few years. The upper left, upper right, lower right and lower left panel is calculated without any magnetic fields, with only the EGMF, with only the GMF and with both magnetic fields respectively.

three sources. When the effects of the EGMF are included (upper right), we find the diffusion of the clustered events. In the lower left panel, the clustered events are arranged in the order of their energies, reflecting the directions of the GMF. This was pointed out by Alvarez-Muniz, Engel & Stanev (2002) and Yoshiguchi et al. (2003b). Note that we cannot find the clustered events at the direction of one of the strong sources $(l, b) = (25^\circ, 11^\circ)$. This is because UHE protons injected at this source cannot reach the earth due to the GMF. In the lower right panel, we also find the arrangements at the same point of the lower left panel. But the EGMF diffuses these clustered events as we see in the two upper panels.

In order to see these features quantitatively, we compare the statistical quantities calculated with the EGMF to those calculated without the EGMF in the presence of the GMF in the next subsection.

5.3. Statistics on the UHECR Arrival Distribution

In this subsection, we compare the statistical quantities calculated with the EGMF to those without the EGMF. We take $n_{\text{source}} \sim 5 \times 10^{-6} \text{ Mpc}^{-3}$.

Figure 10 and figure 11 show the two point correlation function simulated by our source model with $E > 4 \times 10^{19} \text{ eV}$ and $E > 10^{19} \text{ eV}$ respectively. In each figure, the right panel is the two point correlation function calculated with the EGMF and the left panel is that without the EGMF. We calculate the two point correlation function for simulated events within only $-10^\circ \leq \delta \leq 80^\circ$ in order to compare our results with the AGASA data. The shaded regions represent 1σ total statistical error, which is caused by the finite number of simulated events and the random source selections from our IRAS sample. In order to see the effect of each error component on this total error, we also draw an errorbar, which represents the statistical fluctuations due to the finite number of the simulated events, which is set to be equal to that observed by the AGASA (49 events for $E > 4 \times 10^{19} \text{ eV}$ and 775 events for $E > 10^{19} \text{ eV}$). The event selections and the source selections are performed 100 times and 40 time respectively. The histograms represent the AGASA data (Takeda et al. 2001). For the data of $E > 10^{19} \text{ eV}$, we normalize the two point correlation function as the correlation function obtained by the AGASA fits the calculated one at 30° , since we cannot know the normalization of the AGASA data with this energy.

In both figure 10 and 11, it is visible that a peak at small angle is too stronger than that of the AGASA though the calculated two point correlations have very large errors, which are mainly caused by the source selection. In our previous work (Yoshiguchi et al. 2003b), we also faced this situation and pointed out possible explanations, one of which was effects of the EGMF. We find that a peak of two point correlation function calculated with the EGMF at small angle scale is weaker than that without the EGMF. Thus the consistency with the AGASA data becomes better.

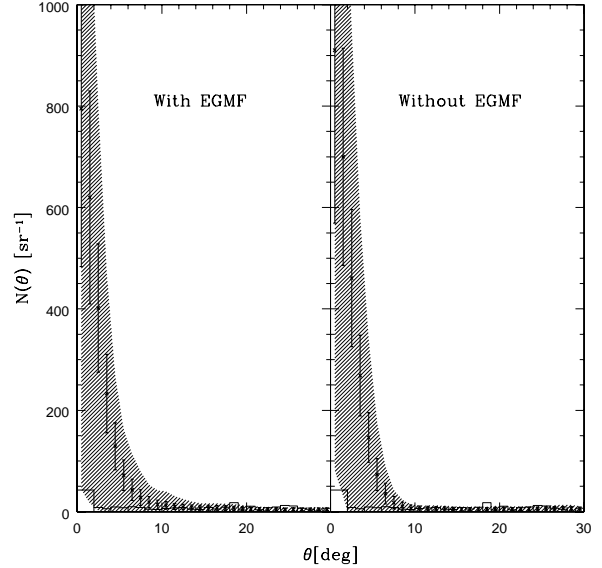


FIG. 10.— Two point correlation function calculated from our source model for $E > 4 \times 10^{19} \text{ eV}$ (49 events). The left panel shows the two point correlation calculated with the EGMF and the right one shows that calculated without the EGMF. The shaded regions represent 1σ total error to consist of statistical error due to the finite number of the simulated events, which is set to be equal to that observed by the AGASA within $-10^\circ < \delta < 80^\circ$, and one due to the source selection. The errorbars represent the statistical fluctuation due to the finite number of the simulated events in order to see this error contribute to the total error. The histograms represent the AGASA data.

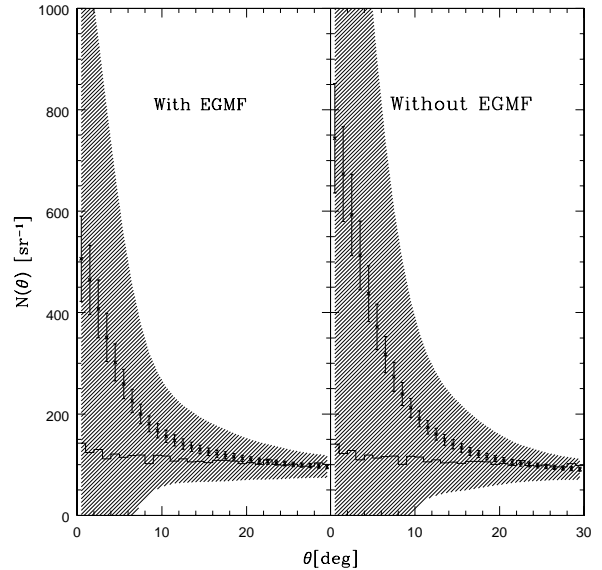


FIG. 11.— Same as figure 10. But this two point correlation is calculated for $E > 10^{19} \text{ eV}$ (775 events within $-10^\circ < \delta < 80^\circ$). However, we fit the AGASA data to that calculated from our source model at $\theta_{\text{max}} = 30^\circ$ since we cannot know the normalization of the AGASA data with this energy range.

As mentioned above, the calculated two point correlation functions have large errors since there are source distributions in our source model which contain sources very near to us. Such source distributions do not explain the large-scale isotropy observed by the AGASA. We check that 11 source distributions out of 40 predict the sufficient large-scale isotropy obtained by

the AGASA within 1σ statistical error due to the finite number of the simulated events. Using these 11 source distributions, we calculate the two point correlation function in the presence of the EGMF. The results are shown in figure 12.

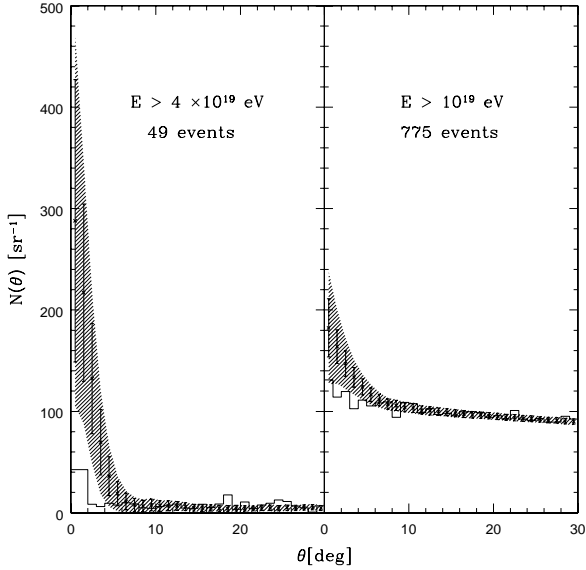


FIG. 12.— Two point correlation function calculated with the EGMF from 11 source distribution which satisfy the large-scale isotropy observed by the AGASA fully, for $E > 4 \times 10^{19}$ eV (49 events, left) and $E > 10^{19}$ eV (775 events, right). These function is calculated within $-10^\circ < \delta < 80^\circ$. The shaded regions and the errorbars have the same mean as figure 10, 11. The histograms represent the AGASA data. The normalization of the AGASA data with $E > 10^{19}$ eV performs the same as figure 11.

Figure 12 shows that the consistency with the AGASA data becomes better than that of the left panels in figure 10 and 11. We also see that the error due to the source selections becomes small since we adopt only source distributions which have the large-scale isotropy consistent with the AGASA within 1σ . However, we should note that the peak at small angle scale is still relatively strong compared with the AGASA though our previous result (Yoshiguchi et al. 2003b) is improved by the effect of the EGMF. We assume effects of the random component of the GMF, which is neglected in this work, as one of possible explanations for this fact since the EGMF improves the consistency with the AGASA in this work. This issues are left for future investigations.

We also investigate the harmonic amplitude in the same way. But there is little difference dependent on the EGMF.

6. SUMMARY AND DISCUSSION

We present numerical simulations on propagation of UHECRs above 10^{19} eV in a structured EGMF and the GMF. We use the IRAS PSCz catalogue in order to construct a structured EGMF model which reflects the local structure actually observed, and source models of UHECRs. We calculate an inverse process of their propagation containing the energy loss

processes in the EGMF. We inject UHECRs from the earth isotropically whose charges are taken as -1 and record these trajectories. They can be regarded as trajectories of UHE protons from the extragalactic space. We then select some of their trajectories according to a given source distribution. The simulated arrival distribution is able to be constructed by mapping the velocity directions of the selected trajectories at the earth. With the use of this method, we can calculate only trajectories of UHECRs reaching the earth and save the CPU time effectively. The validity of this method is supported by Liouville's theorem.

We calculate the harmonic amplitudes and the two point correlation functions of arrival distribution of UHECRs above 10^{19} eV, using our source models and examine what number density of source explains the large-scale isotropy and the small-scale anisotropy obtained by the AGASA best. As a result, we find that $\sim 5 \times 10^{-6}$ Mpc $^{-3}$ is the most appropriate number density of source of UHECRs. Number density of source is a constraint on source candidate of UHECRs.

We also demonstrate skymaps of the arrival distribution of UHECRs above 10^{19} eV, using our source model for $n_{\text{source}} \sim 5 \times 10^{-6}$ Mpc $^{-3}$ with the event number expected by future experiments and examine how the EGMF affects the arrival distribution of UHECRs. The main result is diffusion of clustering events which is obtained by calculations neglecting the EGMF.

In order to see the effect of the EGMF quantitatively, we compare the two point correlation function calculated with our structured EGMF model to the one without the EGMF. We find that the EGMF weakens the small-scale anisotropy and improves a prediction in Yoshiguchi et al. (2003b), which was calculated with only the GMF.

However, the calculated two point correlation functions have large errorbars since source distributions, which contain sources very near to us, exist. Such source distributions do not explain the large-scale isotropy observed by the AGASA. Thus we calculate the two point correlation function using source distributions which predict the large-scale isotropy obtained by the AGASA within 1σ statistical error. This simulated two point correlation function explains that of the AGASA better. It is possible that this function at small angle scale can be closer to the observational data due to the random component of the GMF. This issue is left for future studies.

New large aperture detectors are under development, such as the Pierre Auger observatory (Capelle et al. 1998), the EUSO (Benson & Linsley 1982) and the Telescope Array. These projects are expected to increase observed events of UHECRs per year drastically. We can obtain more strong constraints on our source model, other than number density of source, using other statistical quantities when the detailed data of large events of UHECRs are published. This is one of plans of future study.

The work of H.Y. is supported by Grants-in-Aid for JSPS Fellows. The work of K.S. is supported by Grants-in-Aid for Scientific Research provided by the Ministry of Education, Science and Culture of Japan through Research Grant No.S14102004 and No.14079202.

REFERENCES

Abbasi R.U. et al. (The Hires Collaboration) 2004, ApJ, 610, L73
 Abu-Zayyad T. et al. (The HiRes Collaboration) 2004, Phys. Rev. Lett., 92, 151101
 Aloisio R. & Berezinsky V. 2004, ApJ, 612, 900
 Alvarez-Muniz J., Engel R., & Stanev T. 2002, ApJ, 572, 185
 Beck R. 2001, Space. Sci. Rev. 99, 243
 Benson R., & Linsley J. 1982, A&A, 7, 161
 Berezinsky V., & Grigorieva S.I. 1988, A&A, 199, 1

Bhattacharjee P. & Sigl G. 2000, Phys.Rep., 327, 109

Bieber, J.W, Evenson, P.A & Lin, Z. 1992, Antarctic J., 27, 318

Capelle K.S., Cronin J.W., Parente G. & Zas E. 1998, Astropart.Phys., 8, 321

Chodorowski M.J., Zdziarska A.A., & Sikora M. 1992, ApJ, 400, 181

Dolag K., Bartelmann M. & Lesch H., A&A, 387, 383

Dolag K., Grasso D., Springel V. & Tkachev I., JCAP 0501, 009

Farrar G.R. (The HiRes Collaboration), 2004, astro-ph/0412617

Flückiger et al., Proc. Int. Cosmic Ray Conf.(Dublin), 3, 648

Fusco-Femiano, R. et al. ApJ, 513, L21

Greisen K. 1966, Phys. Rev. Lett., 16, 748

Han J.L., & Qiao G.J. 1994, A&A, 288, 759

Han J.L., Manchester R.N., & Qiao G.J. 1999, MNRAS, 306, 371

Han J.L., 2001, Ap&SS, 278, 181

Han J.L., 2002, astro-ph/0110319.

Hayashida N., et al. 1999 APh, 10, 303

Hayashida N., et al. 2000, AJ, 120 2190

Hillas, A.M. 1984, ARA&A, 22, 425

Marco D.D., Blasi P., & Olinto A.V. 2003, Astropart.Phys., 20, 53

Medina-Tanco G., Topics in Cosmic-Ray Astrophysics: Horizons in World Physics, Vol. 230, Edited by Michael A. DuVernois. Published by Nova Science Publishers, Inc., Commack, New York, 1999, p.287

Mucke A., Engel R., Rachen J.P., Protheroe R.J., & Stanev T. 2000, Comput. Phys. Commun. 124, 290

Rephaeli, Y., Gruber, D., & Blanco, P., 1999, ApJ, 511, L21

Santiago B.X., Strauss M.A., Lahav O., Davis M., Dressler A., & Huchra J.P. 1995, ApJ, 446, 457

Saunders W. et al. 2000, MNRAS 317, 55

Sigl G., Miniati F., & Ensslin T.A. 2003, Phys. Rev. D, 68, 043002

Sigl G., Miniati F., & Ensslin T.A. 2004, Phys. Rev. D, 70, 043007

Stanev T. 1997, ApJ, 479, 290

Takeda M., et al. 1998, Phys. Rev. Lett., 81, 1163

Takeda M., et al. 1999, ApJ, 522, 225

Takeda M., et al. 2001, Proceeding of ICRC 2001, 341

Takeuchi T.T., Yoshikawa K & Ishii T.T 2003 ApJ, 587, L89 and the erratum ApJ, 606, L171

Taylor, G.B., Govoni, F., Allen, S.A., & Fabian, A. C. 2001, MNRAS 326, 2

Vallee J.P., AJ 124, 1322

Vallee J.P., New Astron.Rev., 48, 763

Vogt, C. et al. A&A412, 373

Vogt, C & Ensslin T.A., JKAS, 37, 349

Wilkinson C.R., et al. 1999, APh, 12, 121

Yoshida S., & Teshima M. 1993, Prog. Theor. Phys. 89, 833

Yoshiguchi H., Nagataki S., Tsubaki S., & Sato K. 2003a, ApJ, 586, 1231

Yoshiguchi H., Nagataki S., & Sato K. 2003b, ApJ, 596, 1044

Yoshiguchi H., Nagataki S., & Sato K. 2004, ApJ, 614, 43

Zatsepin G.T., & Kuz'min V.A. 1966, JETP Lett., 4, 78